第 50 卷 第 17 期/2023 年 9 月/中国激光 特邀论文

中国激光

嵌入式二氧化钒超表面对太赫兹谐振模式的动态调控

王磊[1]，李花[1]，王永杰[1]，张彩虹[1,2*]，吴敬波[1,2]，范克彬[1,2]，金飚兵[1,2]，陈健[1,2]，吴培亨[1,2]

[1]南京大学电子科学与工程学院，超导电子学研究所，江苏 南京 210023；

[2]紫金山实验室，江苏 南京 211111

摘要 提出了一种在超表面中嵌入二氧化钒(VO_2)从而对太赫兹波进行动态调控的方法。VO_2在68 ℃左右会发生绝缘体到金属的相变，导致其电导率发生4～5个数量级的显著变化。超表面由一个双开口金属谐振环阵列以及金属环开口处嵌入的VO_2结构组成。仿真结果表明，通过改变VO_2的电导率，太赫兹波可以实现高频与低频之间的谐振模式的切换。值得注意的是，这种模式转换不仅可以在实验中通过直接改变环境温度实现，还可以通过激光和强场太赫兹的泵浦完成。这种多样化的激励为该超表面在实际多场景应用中动态调控太赫兹波提供了参考。

关键词 光电子学；太赫兹；超材料与超表面；二氧化钒；激光泵浦；强场太赫兹

中图分类号 O436 **文献标志码** A **DOI**：10.3788/CJL230636

1 引 言

太赫兹(THz)是频率在0.1 THz到10 THz之间(即处于微波和红外频段之间)的一种电磁波，已被证明在实时成像[1]、安全检测[2]、生物传感[3]等领域具有重要作用。太赫兹频段具有大带宽、高数据传输速率的特点，与传统的通信技术相比具有独特优势，这使得它成为一种颇具吸引力的通信技术，为未来第六代(6G)无线通信系统提供了解决方案[4]。但是，由于相邻的微波和红外光学波段所对应的传统电子学和光学设计方法不易直接拓展应用到太赫兹波段，大大阻碍了太赫兹技术的进一步发展，所以亟须发展一种新型的太赫兹器件和设计方法来解决这一难题。

超材料是由一系列呈周期排布的人工设计的微纳结构组成的，这些微纳结构的尺寸、形状以及分布状态在经过精心设计后可以产生自然材料所不具备的光学响应。其中的二维超材料，即超表面，具有生产工艺简单、加工成本低等特点，近几年正逐步替代超材料成为国内外的研究热点[5-6]。将超表面应用于太赫兹技术，可以打破传统材料对太赫兹技术发展的限制。随着应用需求的不断增加，研究人员已将目光从单一、无源的超表面转移到具有调谐功能的有源超表面上来[7-10]。这些可调超表面往往需要依赖于一些可调材料，如石墨烯[11]、液晶[12]、半导体[13]以及一些相变材料[14]。在光、电、热等外界激励下，这些可调材料的光学性质会发生变化，从而实现功能或性能的动态调节。在太赫兹波段，二氧化钒(VO_2)的电导率在相变温度前后有4～5个数量级的突变[15-20]，可以完成绝缘相到金属相的转变。因此，VO_2是一种非常优秀的可调谐材料。

笔者提出了一种通过在超表面中嵌入VO_2从而对太赫兹波进行动态调控的方法。该超表面单元由双开口金属谐振环以及金属环开口处嵌入的VO_2结构组成。仿真结果表明，通过改变电导率，太赫兹波可以实现高频与低频之间的谐振模式的切换。同时，这种模式转换不仅可以在实验中通过直接改变环境温度实现，还可以通过在飞秒激光和强场太赫兹泵浦下完成。这种多样化的激励为在实际多场景应用中动态调控太赫兹传输提供了借鉴。

2 结构设计与原理

图1(a)展示了笔者设计的超表面单元结构，其由双开口谐振环(金材料)以及在开口处嵌入的长方形VO_2结构组成。具体的结构参数为：周期(P)=120 μm，金属臂长(l)=96 μm，臂宽(d)=6 μm，开口宽度(w)=2 μm。为了提高超表面样品加工的容错，用VO_2完全覆盖开口位置，所以VO_2的尺寸为5 μm×9 μm，略大于开口尺寸。通过反应磁控溅射、刻蚀、光刻等微纳加工技术将超表面图案转移到500 μm厚的Al_2O_3衬底上。图1(b)是制备得到的超表面的光学显微照片。

对VO_2外加激励，使其从绝缘态转变成金属态，在

收稿日期：2023-03-21；**修回日期**：2023-05-08；**录用日期**：2023-05-22；**网络首发日期**：2023-06-05

基金项目：国家重点研发计划(2017YFA0700202，2021YFB2800701)、国家自然科学基金(62222106，61871212，92163216，62071217，62027807，62288101)、中央高校基本科研业务费专项资金

通信作者：*chzhang@nju.edu.cn

此过程中，超表面对太赫兹信号的频率响应不同。图 1(c)是笔者使用电磁仿真软件CST微波工作室对单元结构设置周期边界条件进行模拟仿真的结果，其中太赫兹的电场方向垂直于开口方向(y方向偏振)，太赫兹垂直正入射超表面(z方向)。可以清楚地看到，通过设置VO_2的电导率从10 S/m增大到2×10^5 S/m，超表面的谐振频率从0.75 THz红移至0.5 THz左右，金属臂的开口处近似被填补，整个结构完成了从模式1到模式2的转变。为进一步分析谐振模式的机制，对两个谐振模式频点处的电场分布进行了监测，监测结果如图 1(d)所示。可以看出相变前的模式1是开口处电场增强的磁偶极子共振，而相变后的模式2是金属臂导通后的电偶极子共振，其电场主要分布在上下金属臂区域。

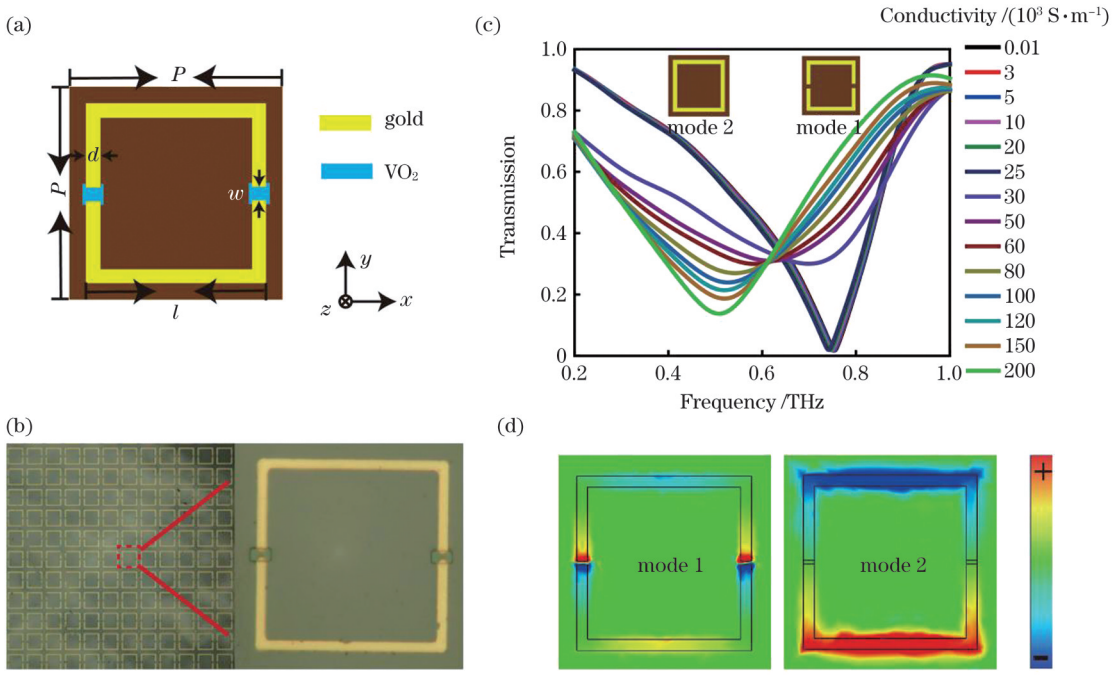

图1 超表面的结构设计及原理示意图。(a)超表面的结构参数和材料示意图；(b)制备的超表面样品的光学显微图；(c)不同VO_2电导率下谐振结构的透射仿真结果；(d)两个模式的电场分布图

Fig. 1 Schematic diagram of the structure design and principle of the metasurface. (a) Schematic diagram of structure parameters and materials of the metasurface; (b) optical micrograph of the prepared metasurface samples; (c) simulation results of transmission of resonator structures under different VO_2 conductivity values; (d) electric field distribution of the two modes

3 分析与讨论

为了验证仿真结果，首先采用传统太赫兹时域光谱系统(THz-TDS)以热激励的方式测试样品的频谱响应。具体做法是：将样品固定在可控温样品架上进行加热，而且样品的开口方向须垂直于太赫兹的电场方向放置。实验结果如图 2所示。当温度低于57 ℃时，结构的谐振频率维持在0.7 THz左右，表明此时的温度变化不会大幅度影响VO_2的电导率，样品处于模式1的状态。随着温度升高，谐振频率逐渐向0.45 THz红移，同时也伴随着谐振峰振幅的逐渐减小，在64 ℃左右谐振峰的振幅达到最小(0.4左右)；继续升高温度，谐振频率继续红移，同时谐振峰的振幅变大，这表明VO_2处于绝缘相与金属相之间的过渡相，超表面处于模式1和模式2之间的过渡态。当温度高于73 ℃时，谐振峰的振幅和谐振频率的变化均不明显，并趋于稳定，此时VO_2电导率趋于饱和，完成了金属臂缺口的填补，表明超表面处于模式2状态。可见，通过直接对样品加热的方式，可使开口连接处的导电通道成功构建，完成超表面从谐振模式1到模式2的转变。图 2(b)是共振频率随温度的变化曲线，该曲线更加直观、定量地反映了温度改变引起的共振频率的动态切换过程。

除了直接对样品进行加热外，笔者还用飞秒激光对样品进行了泵浦。在泵浦实验中采用的是中心波长为800 nm的泵浦脉冲，其对应的光子能量为1.55 eV，大于VO_2处于绝缘相时的带隙能量(为0.67 eV)。VO_2发生相变需要激励光的能流密度达到一定阈值[21]，测得经过透镜的激光在样品处的最大功率为1.3 W。为了使超表面的太赫兹频谱响应在室温和最大光泵浦功率下几乎不发生改变，笔者仿照本课题组先前的做法[17]，将样品加热到VO_2相变温度附近，降低光激发能流密度的阈值。图 3是超表面在相同环境温度和不同激光功率泵浦下的太赫兹透射谱线。图 3(a)是样品在50 ℃下的测量结果，可见：随着激光功率从0 W增大到0.7 W，超表面样品对太赫兹的频率响应无明显

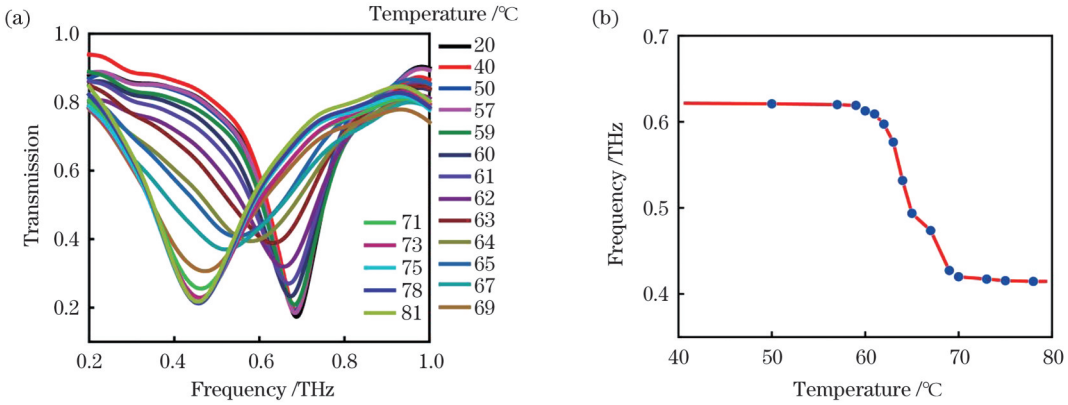

图 2 不同温度下样品的频谱响应。(a)在 20~81 ℃环境温度范围内测得的样品的太赫兹透射谱线;(b)共振频率随温度的变化

Fig. 2 Spectral response of the sample at different temperatures. (a) Terahertz transmission spectra of the samples measured at ambient temperatures of 20–81 ℃; (b) variation of resonant frequency with temperature

变化;随着激光功率由 0.7 W 继续增大到 1.2 W,共振模式的振幅略微减小,共振频率略微红移。这说明超表面处于模式 1。图 3(b)是样品在 60 ℃下的测量结果,此时的温度接近 VO_2 材料的相变温度。随着激光功率从 0 W 增大到 1.3 W,共振频率很明显地从 0.7 THz 红移至 0.45 THz,同时伴随着振幅的变化。这意味着超表面在飞秒激光的泵浦下从模式 1 切换至模式 2。同样,如图 3(c)所示,样品在 62 ℃下也可以完成模式的切换,与图 3(b)不同的是模式 1 的振幅略小。图 3(d)是样品在 70 ℃下的测量结果,此时,VO_2 的电导率已经达到极值,所以随着激光功率的改变,超表面始终稳定在模式 2,共振模式的变化不明显。

可见,通过飞秒激光泵浦也可以改变 VO_2 材料的电导率使其发生相变,从而改变超表面的谐振模式。但值得注意的是,激光泵浦下 VO_2 的相变机制并不是单纯的热效应。激光作用后,V^{4+} 的 3d 价带数减少,产生空穴,从而导致 VO_2 结构带隙闭合并引起能带坍塌。此过程需要达到相变前绝缘晶格与相变后金属晶格之间约 6 THz 的跃迁声子的临界密度,才能支持 VO_2 完成 Mott-Peierls 相变[17,22]。

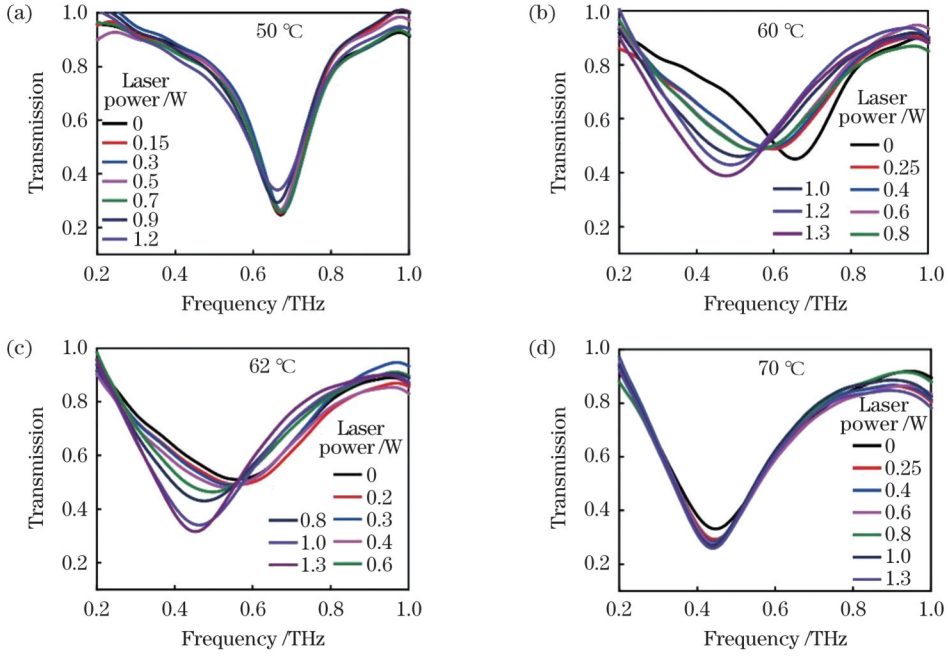

图 3 超表面在相同温度和不同激光功率泵浦下的太赫兹透射谱线。(a) 50 ℃;(b) 60 ℃;(c) 62 ℃;(d) 70 ℃

Fig. 3 Measured terahertz transmission spectra of the metasurface at the same ambient temperature with different laser pump powers. (a) 50 ℃; (b) 60 ℃; (c) 62 ℃; (d) 70 ℃

为了对比飞秒激光泵浦样品的实验,笔者进行了利用飞秒激光泵浦铌酸锂晶体,通过光整流效应产生的强太赫兹场对样品进行泵浦的实验。具体的实验光路如图 4(a)所示。为了控制输出强太赫兹场的强度及偏振,在光路中加入了一对线栅(虚线位置)。理论上,出射太赫兹场的大小与线栅夹角余弦的平方成正比,偏振方向由后一个线栅控制,具体的细节如图 4(b)所示。测得样品处的初始太赫兹电场强度的大小 E_0

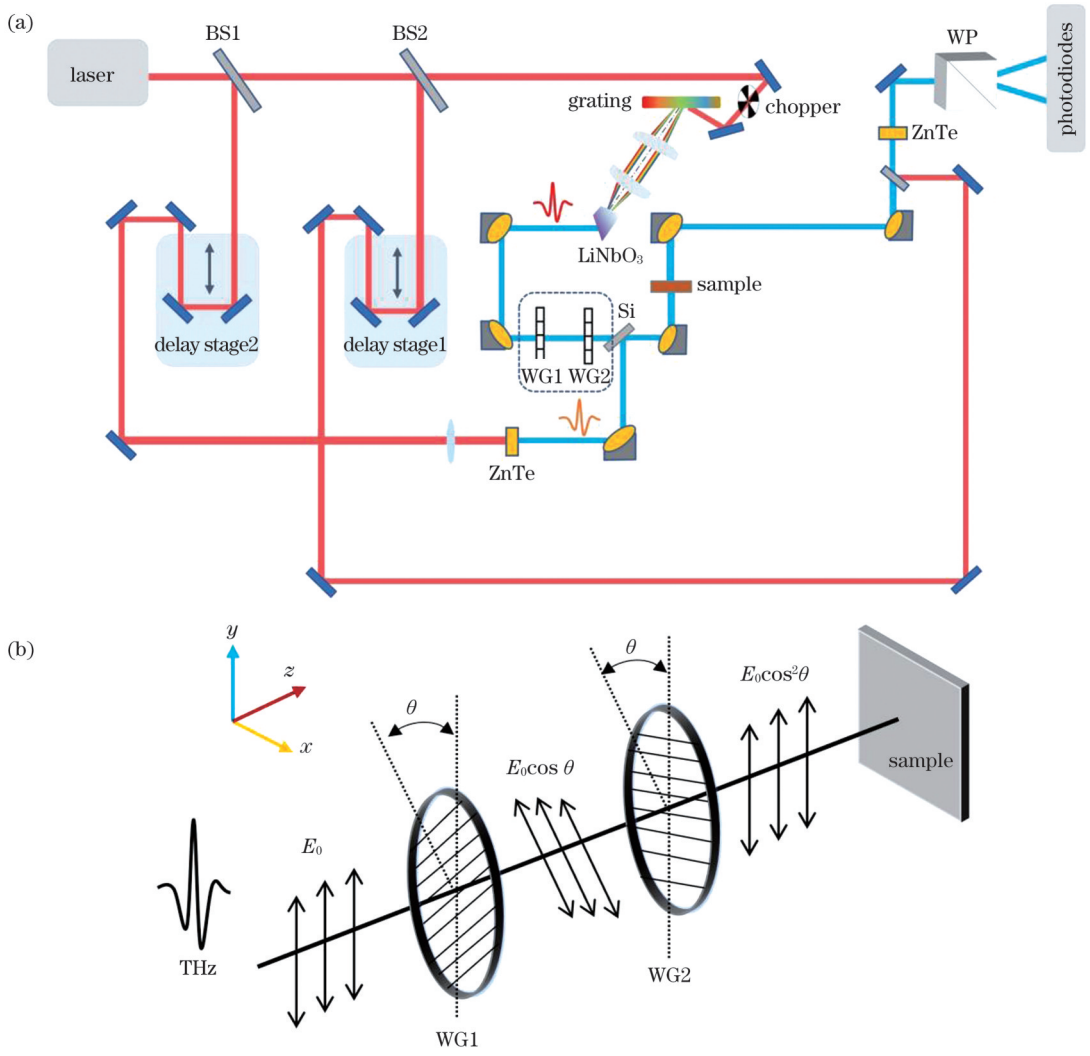

图 4 强太赫兹泵浦-太赫兹探测实验光路示意图及太赫兹线栅细节图。(a)实验光路示意图(BS:分束镜;WG:线栅;WP:沃拉斯顿棱镜);(b)太赫兹线栅细节图

Fig. 4 Schematic diagram of the optical path of the strong THz pump-THz detection experiment and THz wire grid detail diagram. (a) Schematic diagram of the optical path (BS: beam splitter; WG: wire grid; WP: Wollaston prism); (b) THz wire grid detail diagram

约为 100 kV/cm,光斑半径为 1.5 mm。表 1 列出了实验中选取的线栅角度及其与太赫兹强度的对应关系,同时图 5 给出了不同太赫兹强度下衬底基片的透射谱线。该实验光路可以分别完成 1/8、1/4、1/2、3/4 倍初始太赫兹电场强度的强场太赫兹泵浦实验。

同样,将样品升温至其相变附近的温度,不同太赫兹电场作用下的频谱响应结果如图 6 所示。图 6(a)是样品处于 20 ℃时的测量结果,可以看出不同强度的太赫兹激励的透射谱线基本不变,这与激光泵浦测试结果相同。由于 20 ℃远低于 VO_2 的相变温度,太赫兹泵浦的能流密度低于相变阈值,此时超表面处于模式 1。图 6(b)是样品处于 62 ℃时的测量结果,此时的温度接近 VO_2 材料的相变温度,随着太赫兹场强逐渐增大,共振频率很明显地从 0.7 THz 红移至 0.6 THz,同时伴随着振幅的略微减小。这意味着超表面在太赫兹的泵浦下处于从模式 1 切换至模式 2 的过渡态。图 6(c)与图 6(b)的结果类似。值得注意的是,尽管 VO_2 处于相变温度附近,但在强太赫兹场激励下,其并不能完全实现与温度、激光泵浦激励一样的宽频带调控。图 6(d)是样品处于 70 ℃时的测量结果,此时 VO_2 的电导率已经达到极值,随着太赫兹场强增大,共振模式的变化并不明显,超表面始终稳定在模式 2。可见,强太赫兹电

表 1 实验中转动线栅的角度选择与太赫兹强度的对应关系

Table 1 Correspondence between angle of the wire grid and THz amplitude in the experiment

Theta /(°)	Amplitude of THz
68	$0.125E_0$
60	$0.25E_0$
45	$0.5E_0$
30	$0.75E_0$
0	E_0

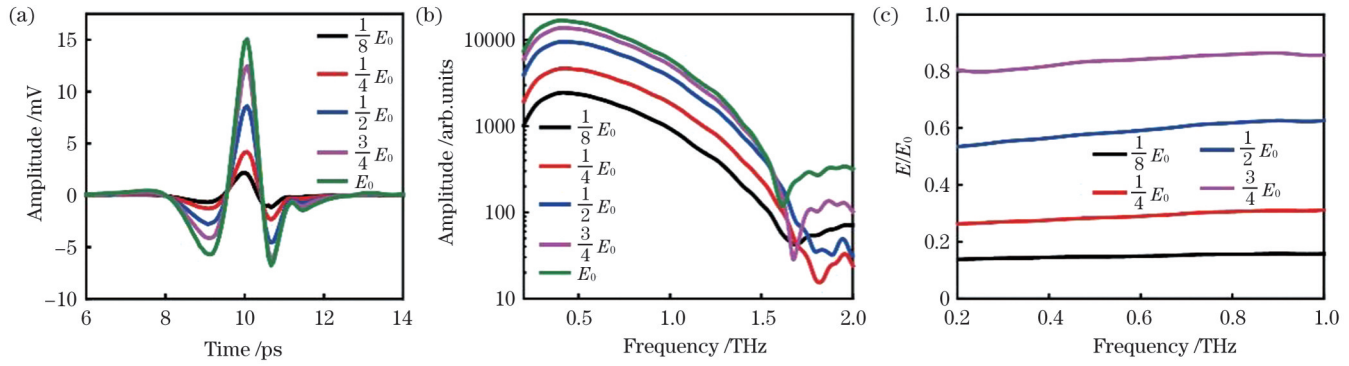

图 5 不同太赫兹强度下基片的太赫兹透射谱线。(a)时域图;(b)频域图;(c)E/E_0图

Fig. 5 Terahertz transmission spectra of the substrate under different intensities of terahertz field. (a) Time-domain diagram; (b) frequency domain diagram; (c) E/E_0 diagram

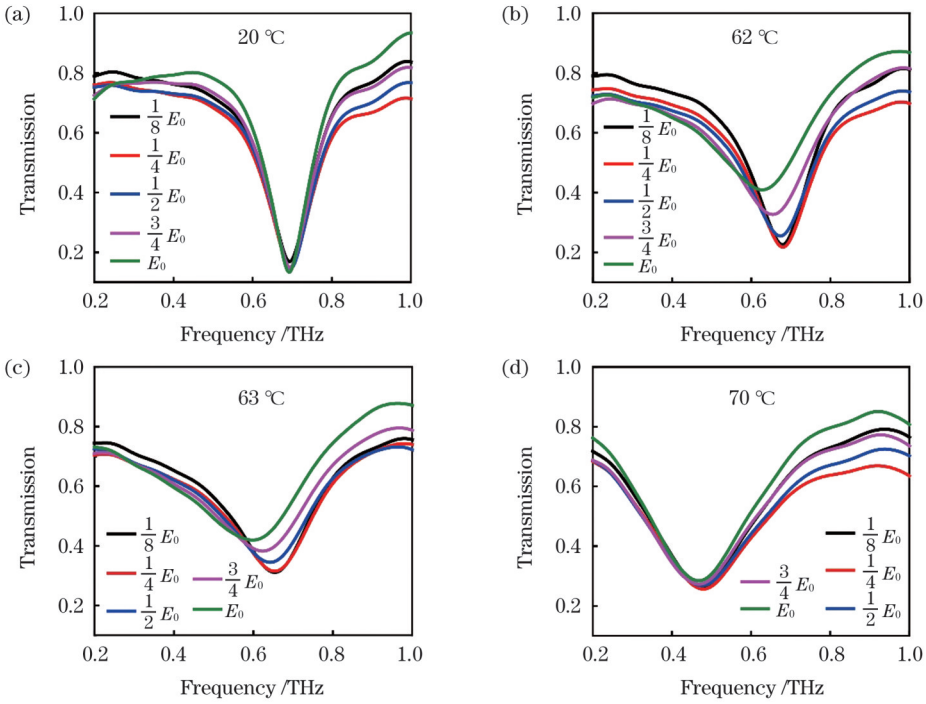

图 6 超表面在同一环境温度和不同太赫兹强度下的太赫兹透射谱线。(a) 20 ℃;(b) 62 ℃;(c) 63 ℃;(d) 70 ℃

Fig. 6 Terahertz transmission spectra of the metasurface at the same ambient temperature and different terahertz field amplitudes. (a) 50 ℃; (b) 62 ℃; (c) 63 ℃; (d) 70 ℃

场可以在一定程度上实现对超表面样品太赫兹电磁响应的控制。

4 结 论

本文提出了一种可调谐嵌入式VO_2超表面,实现了太赫兹波段从高频 0.7 THz 左右到低频 0.43 THz 左右谐振模式的动态切换。谐振环开口处的VO_2在相变前后的电导率经历了 4 个数量级以上的突变,构建了谐振环金属臂的导电通道,从而完成了模式切换。在实验中,通过外加热、激光及强场太赫兹等多种方式的外加激励验证了这种模式切换的可行性。尽管前者与后两者的物理机制有所不同,但多种方式动态激励操控太赫兹波为多场合实际应用提供了借鉴。

参 考 文 献

[1] Guerboukha H, Nallappan K, Skorobogatiy M. Toward real-time terahertz imaging[J]. Advances in Optics and Photonics, 2018, 10(4): 843-938.

[2] Jornet J M, Knightly E W, Mittleman D M. Wireless communications sensing and security above 100 GHz[J]. Nature Communications, 2023, 14: 841.

[3] Zhang C H, Liang L J, Ding L A, et al. Label-free measurements on cell apoptosis using a terahertz metamaterial-based biosensor[J]. Applied Physics Letters, 2016, 108(24): 241105.

[4] Nagatsuma T, Ducournau G, Renaud C C. Advances in terahertz communications accelerated by photonics[J]. Nature Photonics, 2016, 10(6): 371-379.

[5] Hu J E, Bandyopadhyay S, Liu Y H, et al. A review on metasurface: from principle to smart metadevices[J]. Frontiers in Physics, 2021, 8: 586087.

[6] Ali A, Mitra A, Aïssa B. Metamaterials and metasurfaces: a review from the perspectives of materials, mechanisms and advanced metadevices[J]. Nanomaterials, 2022, 12(6): 1027.

[7] He Q, Sun S L, Zhou L. Tunable/reconfigurable metasurfaces: physics and applications[J]. Research, 2019, 2019: 1849272.
[8] Fan K B, Padilla W J. Dynamic electromagnetic metamaterials[J]. Materials Today, 2015, 18(1): 39-50.
[9] 丛龙庆. 主动式太赫兹超材料器件综述[J]. 中国激光, 2021, 48(19): 1914003.
Cong L Q. Active terahertz metadevices[J]. Chinese Journal of Lasers, 2021, 48(19): 1914003.
[10] Fan K B, Averitt R D, Padilla W J. Active and tunable nanophotonic metamaterials[J]. Nanophotonics, 2022, 11(17): 3769-3803.
[11] Miao Z Q, Wu Q, Li X, et al. Widely tunable terahertz phase modulation with gate-controlled graphene metasurfaces[J]. Physical Review X, 2015, 5(4): 041027.
[12] Shrekenhamer D, Chen W C, Padilla W J. Liquid crystal tunable metamaterial absorber[J]. Physical Review Letters, 2013, 110(17): 177403.
[13] Chen H T, Padilla W J, Zide J M O, et al. Active terahertz metamaterial devices[J]. Nature, 2006, 444(7119): 597-600.
[14] Jeong Y G, Bahk Y M, Kim D S. Dynamic terahertz plasmonics enabled by phase-change materials[J]. Advanced Optical Materials, 2020, 8(3): 1900548.
[15] Zhu H F, Du L H, Li J A, et al. Near-perfect terahertz wave amplitude modulation enabled by impedance matching in VO_2 thin films[J]. Applied Physics Letters, 2018, 112(8): 081103.
[16] Chen B W, Wu J B, Li W L, et al. Programmable terahertz metamaterials with non-volatile memory[J]. Laser & Photonics Reviews, 2022, 16(4): 2100472.
[17] Zhang C H, Zhou G C, Wu J B, et al. Active control of terahertz waves using vanadium-dioxide-embedded metamaterials[J]. Physical Review Applied, 2019, 11(5): 054016.
[18] 崔琦, 陈哲, 王岩. 基于二氧化钒超材料的太赫兹波相位动态调控[J]. 中国激光, 2022, 49(3): 0314001.
Cui Q, Chen Z, Wang Y. Dynamic manipulation of terahertz wave phase based on vanadium dioxide metamaterials[J]. Chinese Journal of Lasers, 2022, 49(3): 0314001.
[19] 黄成成, 张永刚, 梁兰菊, 等. 窄/宽带可切换的石墨烯-二氧化钒复合结构太赫兹吸波器[J]. 光学学报, 2022, 42(19): 1916001.
Huang C C, Zhang Y G, Liang L J, et al. Narrow/broadband switchable graphene-vanadium dioxide composite structure terahertz wave absorber[J]. Acta Optica Sinica, 2022, 42(19): 1916001.
[20] 张婷, 杨森, 于新颖. 基于二氧化钒的可调宽带太赫兹完美吸收器设计[J]. 激光与光电子学进展, 2021, 58(21): 2116002.
Zhang T, Yang S, Yu X Y. Tunable broadband terahertz perfect absorber design based on vanadium dioxide[J]. Laser & Optoelectronics Progress, 2021, 58(21): 2116002.
[21] Hilton D J, Prasankumar R P, Fourmaux S, et al. Enhanced photosusceptibility near t_c for the light-induced insulator-to-metal phase transition in vanadium dioxide[J]. Physical Review Letters, 2007, 99(22): 226401.
[22] Cocker T L, Titova L V, Fourmaux S, et al. Phase diagram of the ultrafast photoinduced insulator-metal transition in vanadium dioxide[J]. Physical Review B, 2012, 85(15): 155120.

Dynamic Modulation of Terahertz Resonance Modes by Embedded Vanadium Dioxide Metasurfaces

Wang Lei[1], Li Hua[1], Wang Yongjie[1], Zhang Caihong[1,2*], Wu Jingbo[1,2], Fan Kebin[1,2], Jin Biaobing[1,2], Chen Jian[1,2], Wu Peiheng[1,2]

[1]*Research institute of Superconductor Electronics (RISE), School of Electronic Science and Engineering, Nanjing University, Nanjing* 210023, *Jiangsu, China*;

[2]*Purple Mountain Laboratories, Nanjing* 211111, *Jiangsu, China*

Abstract

Objective Terahertz (THz) is a electromagnetic wave with the frequency range of 0.1-10 THz, and is gradually playing an important role in many fields. However, because traditional electronic and optical design methods consider the adjacent microwave and infrared optical bands, the application of the THz band is not easy to directly expand, which will undoubtedly greatly hinder further development of THz technology. Thus, there is an urgent need for new THz device design methods to solve this difficulty. Metamaterials are composed of a series of micro- and nanostructures with artificially designed periodic arrangements, whose size, shape, and distribution can produce optical responses that natural materials do not exhibit after careful design. Two-dimensional metamaterials, i. e., metasurfaces, with a simple process flow and low processing cost, have gradually replaced metamaterials in recent years and have become a popular research topic. The application of metasurfaces to THz technology overcomes the limitations of traditional materials, contributing to their development. With the increasing demand for corresponding applications, researchers have shifted their attention from single passive hypersurfaces to tunable active metasurfaces. These tunable metasurfaces are often dependent on several tunable materials. In particular, in the THz band, vanadium dioxide (VO_2) is an excellent tunable material that is being actively investigated by researchers due to its abrupt change in conductivity of four to five orders of magnitude before and after the phase transition temperature, which allows it to complete the insulating to the metallic phase transition.

Methods A metasurface comprising a periodic array of double-gap split-ring resonators, with VO_2 structures embedded in the gaps, was considered in this study. The spectral responses to different VO_2 conductivities and electric field distribution images of the corresponding modes were first simulated using the commercial simulation software, CST. Next, samples were obtained via conventional lithography and other micro- and nano-processing techniques, which were then characterized experimentally using THz time-domain spectroscopy (TDS). First, the samples were heated directly using a hot stage, followed by laser pumping, strong THz pumping, and THz detection for mode characterization.

Results and Discussions The simulation results clearly show that with increasing VO_2 conductivity from 10 to 2×10^5 S/m, the resonant frequency red-shifts from 0.75 to approximately 0.5 THz, the gap of the metal arm is approximately filled, and the whole structure completes the transition from mode 1 to mode 2. Field monitoring shows that before the phase transition, mode 1 is a magnetic dipole resonance with an enhanced electric field at the opening; whereas, after the phase transition, mode 2 is an electric dipole resonance after the conduction of the metal arm, and its electric field is mainly distributed in the upper and lower metal arm regions (Fig. 1). Direct characterization of the sample heating confirmed the simulation results. At temperatures lower than 57 ℃, the resonant frequency of the structure remained at approximately 0.7 THz, indicating that the temperature change at this time could not substantially affect the conductivity of VO_2, and the sample was in the mode 1 state. As the temperature increases further, the resonant frequency gradually red-shifts to 0.45 THz, accompanied by a gradual decrease in the amplitude of the resonant peak, reaching a minimum of approximately 0.4 at ~64 ℃. With continuing increase in temperature, the resonant frequency continues to red-shift, and the amplitude becomes larger, indicating that VO_2 is transitioning between the insulating phase and the metallic phase. For temperatures higher than 73 ℃, the resonance mode does not change significantly in both amplitude and resonance frequency, and tends to stabilize, at which time the VO_2 conductivity tends to saturate and completes the filling of the metal arm gap, indicating that the metasurface is in the state of mode 2. Therefore, by directly heating the sample, a conductive channel at the gap is successfully constructed, the transition from resonant mode 1 to mode 2 of the metasurface is completed, and the variation in the resonant frequency with temperature provides a more direct reflection of the mode switching (Fig. 2). Laser pumping requires heating the respective sample to near the phase transition temperature; similarly, different laser powers can induce a VO_2 phase transition (Fig. 3). Finally, strong THz pumping of samples with different intensities can also produce the VO_2 phase change. It is worth noting that although VO_2 is in the vicinity of the phase transition temperature, broadband modulation, such as temperature and laser pumping excitation, cannot be fully achieved under strong THz field excitation (Figs. 5 and 6).

Conclusions In this paper, a tunable, embedded VO_2 hybrid metasurface is proposed to realize the dynamic switching of resonant modes from a high frequency of around 0.7 THz to a low frequency of around 0.43 THz in the THz band. The VO_2 at the opening of the resonant ring undergoes a sudden change in conductivity by more than four orders of magnitude before and after the phase transition, constructing a conductive channel in the metal arm of the resonant ring and thus completing mode switching. The feasibility of this mode-switching was verified experimentally through various applications of thermal, laser, and strong-field THz excitations. Although the physical mechanisms of the former and latter two differ, the multimode dynamic excitation manipulation of THz waves presents a feasible idea for practical applications.

Key words optoelectronics; terahertz; metamaterial and metasurface; vanadium dioxide; laser pump; strong-field terahertz